Rate-splitting multiple access in satellite-terrestrial communication systems: performance analysis

Huu Q. Tran[1], Khuong Ho-Van[2]

[1]Department of Electronics and Telecommunication, Faculty of Electronics Technology, Industrial University of Ho Chi Minh City, Ho Chi Minh City, Vietnam

[2]Department of Telecommunication Engineering, Faculty of Electrical and Electronics Engineering, Ho Chi Minh City University of Technology (HCMUT), VNU-HCM, Ho Chi Minh City, Vietnam

Article Info

ABSTRACT

This paper investigates the throughput and outage probability (OP) of rate-splitting multiple access (RSMA) in satellite–terrestrial communication networks. By dividing user messages into common and private parts, RSMA enhances spectral efficiency and user fairness while addressing hardware impairments and co-channel interference. The proposed hybrid system model is analyzed and compared with non-orthogonal multiple access (NOMA) under various power allocation coefficients and channel conditions. Results show that RSMA achieves lower OP and higher throughput than NOMA, particularly in dense multi-cell deployments. Numerical evaluations further demonstrate RSMA's robustness against interference and hardware limitations, underscoring its potential as a reliable solution for next-generation satellite–terrestrial relay networks.

Corresponding Author:

Huu Q. Tran
Department of Electronics and Telecommunication, Faculty of Electronics Technology
Industrial University of Ho Chi Minh City
Go Vap District, Ho Chi Minh City, Vietnam
Email: tranquyhuu@iuh.edu.vn

1. INTRODUCTION

In rapidly evolving landscape of wireless communication, achieving higher spectral efficiency, energy efficiency, and reliability is crucial to addressing the rising demand for seamless and ubiquitous connectivity. The exponential growth of devices connected to the Internet, combined with the ever-increasing demands for data-intensive applications, underscores the need for innovative multiple access techniques capable of overcoming the limitations of conventional schemes. Among these advanced techniques, rate-splitting multiple access (RSMA) becomes a feasible candidate for 6G networks and beyond, poised to redefine the paradigms of wireless communication [1]-[5]. RSMA leverages an intelligent and adaptive approach to interference management by dividing user signals into common and private components, enabling a more granular and effective handling of inter-user interference [6], [7]. Unlike traditional schemes, RSMA empowers receivers to implement flexible signal decoding strategies through successive interference cancellation (SIC). This allows partial decoding of interference whilst considering the residual interference as noise, leading to more robust communication performance in diverse network conditions [3], [8], [9]. Such flexibility makes RSMA uniquely suitable for scenarios characterized by heterogeneous user channel conditions and non-ideal propagation environments,

where conventional techniques like non-orthogonal multiple access (NOMA) and orthogonal multiple access (OMA) struggle to maintain reliability consistency [10], [11]. Furthermore, the adoption of RSMA isn't constrained to terrestrial communication networks yet widens to satellite-terrestrial communication systems, where unique challenges such as long propagation delays, limited spectrum, and coexistence of multiple service layers create a complex operational environment [12]-[14]. The integration of RSMA in satellite-terrestrial networks enhances resource utilization and interference management, addressing traditional performance bottlenecks. These networks are crucial for next-generation wireless infrastructure, supporting wide-area coverage, high data rates, and low latency, especially in remote or under served regions. They also provide robust support during peak demand and for disaster recovery. However, they face challenges like severe co-channel interference, dynamic user distributions, and stringent quality-of-service (QoS) requirements [15], [16]. The escalating demand for satellite-terrestrial connectivity, driven by emerging technologies like 6G, the Internet of Things (IoT), and disaster recovery systems, has intensified the urgency to address these challenges. By 2030, the quantity of IoT devices is estimated to be over 30 billion, while 6G networks will require ultra-reliable low-latency (URLL) communications to support mission-critical applications [17]. Additionally, satellite-terrestrial systems are vital for ensuring connectivity during natural disasters, where terrestrial infrastructure may be compromised [15]. However, conventional multiple access schemes like NOMA and orthogonal multiple access (OMA) struggle to meet these demands due to their limited ability to manage severe co-channel interference and dynamic user distributions effectively. NOMA, while improving spectral efficiency, often fails to ensure fairness among users with heterogeneous channel conditions [2], and OMA's orthogonal resource allocation leads to suboptimal spectrum utilization [10]. These limitations result in degraded QoS, particularly in scenarios requiring high reliability and low latency, underscoring the need for advanced techniques like RSMA to bridge the performance gap. RSMA's ability to split signals into common and private streams offers a transformative approach, improving spectral efficiency, energy utilization, and fairness among users, even with heterogeneous channel conditions and unpredictable interference. This makes RSMA particularly beneficial for optimizing the throughput of satellite-terrestrial communication networks. Nevertheless, the deployment of RSMA in satellite-terrestrial communications networks has not been thoroughly explored, resulting in a lack of crucial insights needed to achieve QoS standards. The rapid expansion of connected devices and data intensive applications, expected to grow significantly by 2030 [17], underscores the critical need for robust satellite-terrestrial communication systems to ensure seamless connectivity in remote and underserved regions. Conventional multiple access schemes, such as NOMA and OMA, face significant challenges due to co-channel interference and dynamic user distributions, limiting their ability to meet stringent QoS requirements. Moreover, satellite communications also face environmental impairments such as rain attenuation, which can significantly degrade link reliability in multibeam satellite systems [18]. In parallel, cooperative relaying with energy harvesting has been investigated as a promising solution to enhance both security and reliability in future wireless networks, despite the presence of hardware impairments [19]. These studies highlight the importance of considering both environmental and hardware constraints when designing robust satellite–terrestrial multiple access systems.

To bridge this gap, our paper continues to contribute to this field with the key contributions itemized as follows: (i) we derive mathematical expressions for outage probability (OP) and conduct asymptotic analysis to evaluate system performance comprehensively and (ii) this study evaluates the influence of power distribution factors and the quantity of satellite antennas on the overall reliability and dependability of the system. The subsequent section describes RSMA in satellite-terrestrial communication systems. Subsequently, section 3 performs the OP analyses. Section 4 discusses the simulated and analytical results under various practical settings. Eventually, section 5 presents conclusions.

2. RSMA IN SATELLITE-TERRESTRIAL COMMUNICATION SYSTEMS

2.1. System model

This subsection provides an overview of RSMA in wireless communications, covering both satellite and terrestrial systems, as in Figure 1. A satellite with K antennas communicates with Q terrestrial users using RSMA to serve all users simultaneously. Modern satellite communications often uses multi-beam technology to enhance spectral efficiency, especially in geosynchronous earth orbit (GEO) satellites, where array-fed reflectors generate multiple beams more efficiently than direct radiation arrays. This setup fixes each beam's radiation pattern, reducing the need for complex on-board processing. However, achieving accurate channel state information (CSI) is challenging because of erroneous channel estimation. Techniques like the linear

minimal mean square error method are used to predict CSI, yielding the combined channel coefficient between S and the qth user as:

$$\mathbf{h}_{U_q} = \left(\mathbf{g}_{U_q}^\dagger \mathbf{w}_{U_q} + e_{U_q} \right) \sqrt{L_{SU_q} \vartheta_S \vartheta \left(\theta_{U_q} \right)} \tag{1}$$

where $\mathbf{w}_{U_q}$ is $K \times 1$ transmit weight vector, e_{U_q} means channel estimation error with $e_{U_q} \sim \mathcal{CN} \left(0, \mu_{U_q}^2 \right)$, ϑ_S is satellite antenna gain, $\mathbf{g}_{U_q}$ is the estimated $K \times 1$ shadowed-Rician channel coefficient vector between K antennas at S and the qth user, and $(.)^\dagger$ denotes conjugate transpose. The transmit beamforming vector $\mathbf{w}_{U_q} \in \mathbb{C}^{K \times 1}$ is selected in accordance with the maximum ratio transmission (MRT) principle, given that $\mathbf{w}_{U_q} = \frac{\|\mathbf{g}_{U_q}\|}{\|\mathbf{g}_{U_q}\|_F}$ in which $\|.\|_F$ denotes the Frobenius norm. Moreover, $L_{SU_q} = \frac{1}{\mathcal{K}_B TW} \left(\frac{c}{4\pi f_c d_{SU_q}} \right)^2$ means instantaneous free space loss [20] wherein d_{SU_q} is distance between S and U_q, f_c is carrier frequency, W is transmission bandwidth, T is noise temperature at the receiver, $\mathcal{K}_B = 1.38 \times 10^{-23} J/K$ is Boltzmann constant, c is speed of light. Furthermore, the satellite's beam gain $\vartheta \left(\theta_{U_q} \right)$ is expressed to be:

$$\vartheta \left(\theta_{U_q} \right) = \vartheta_{U_q} \left(\frac{I_1 \left(\bar{\rho}_{U_q} \right)}{2\bar{\rho}_{U_q}} + 36 \frac{I_3 \left(\bar{\rho}_{U_q} \right)}{\bar{\rho}_{U_q}^3} \right) \tag{2}$$

where θ_{U_q} is the angular separation, ϑ_{U_q} is the antenna gain at U_q, I_i is the first-kind Bessel function with order i, $\bar{\rho}_{U_q} = 2.07123 \frac{\sin \theta_{U_q}}{\sin \theta_{U_q 3\text{dB}}}$ in which $\sin \theta_{U_q 3\text{dB}}$ represents 3 dB beamwidth.
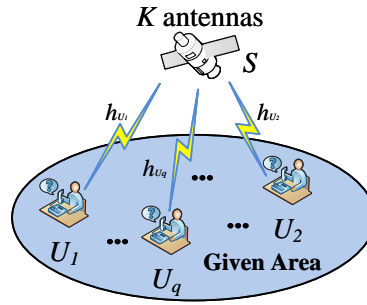

Figure 1. The considered system model

2.2. Signal processing at transceivers

This research employs RSMA signaling at the transmitter to facilitate concurrent communication with all recipients. RSMA operates by dividing the transmitted information into a shared signal (x_c) distributed across all recipients and personalized messages tailored for each recipient. The transmitter designates a power distribution factor (a_c) for the shared signal, with the residual power assigned to the personalized messages. Subsequently, it transmits a composite of the shared and personalized messages to the recipients.

$$x = \sqrt{P_S} \left(\sqrt{a_c} x_c + \sum_{q=1}^{Q} \sqrt{a_q} x_q \right) \tag{3}$$

wherein P_S represents the power allocated at S for downlink communication, and x_q signifies the private message designated for the qth user, accompanied by a power allocation coefficient denoted as a_q. It is important to note that $a_c + \sum_{q=1}^{Q} a_q = 1$.

The ith user obtains the signal articulated to be:

$$y_{U_q} = \mathbf{h}_{U_q} x + n_{U_q} = \underbrace{\left(\mathbf{g}_{U_q}^\dagger \mathbf{w}_{U_q} + e_{U_q} \right) \sqrt{L_{SU_q} \vartheta_S \vartheta \left(\theta_{U_q} \right) a_c P_S} x_c}_{\text{Common Message}} + \underbrace{\left(\mathbf{g}_{U_q}^\dagger \mathbf{w}_{U_q} + e_{U_q} \right) \sqrt{L_{SU_q} \vartheta_S \vartheta \left(\theta_{U_q} \right) a_q P_S} x_q}_{\text{Desired Private Message}}$$

$$+ \underbrace{\left(\mathbf{g}_{U_q}^\dagger \mathbf{w}_{U_q} + e_{U_q} \right) \sum_{j=1, q \neq j}^{Q} \sqrt{L_{SU_q} \vartheta_S \vartheta \left(\theta_{U_q} \right) a_j P_S} x_j}_{\text{Interfernce}} + \underbrace{n_{U_q}}_{\text{AWGN}}$$

$$\tag{4}$$

wherein n_{U_q} represents zero-mean σ_q^2-variance additive white Gaussian noise (AWGN). The (4) clearly unveils that each user receives not only private and common information dedicated to itself but also private information intended for other users, yielding interference when recovering information. To mitigate this, each user conducts a two-stage restoring process to retrieve expected messages from its received signal. By considering all other data as noise, shared information is retrieved in the initial phase. The signal-to-noise-plus-interference ratio (SINR) for extracting the shared signal at the qth recipient measures how effectively the recipient can isolate the communal data amidst disruptions from personalized messages designated for other recipients. This SINR reflects the power assigned to the shared signal, channel characteristics (including antenna gains and free space loss), and the effects of channel estimation inaccuracies and ambient noise. A higher SINR signifies improved decoding reliability for the shared signal, which is essential for RSMA's interference mitigation approach. Consequently, the qth recipient retrieves shared information with SINR as:

$$\bar{\gamma}_{c,q} = \frac{a_c L_{SU_q} \vartheta_S \vartheta\left(\theta_{U_q}\right) P_S \left\|\mathbf{g}_{U_q}\right\|_F^2}{L_{SU_q} \vartheta_S \vartheta\left(\theta_{U_q}\right) P_S \left(1 - a_c\right) \left\|\mathbf{g}_{U_q}\right\|_F^2 + L_{SU_q} \vartheta_S \vartheta\left(\theta_{U_q}\right) P_S \mu_{U_q}^2 + \sigma_q^2} = \frac{a_c \mathcal{A}_q}{\left(1 - a_c\right) \mathcal{A}_q + \delta_q \mu_{U_q}^2 + 1}$$

(5)

wherein $\varrho_S = P_S / \sigma_q^2$ is transmit signal-to-noise radio (SNR), $\mathcal{A}_q = \delta_q \left\|\mathbf{g}_{U_q}\right\|_F^2$ and $\delta_q = \varrho_S L_{SU_q} \vartheta_S \vartheta\left(\theta_{U_q}\right)$. Upon the successful decryption of the shared message, the subsequent stage entails each user extracting its intended private information by deducting the recovered shared information from the received signal whereas presuming the private information from all other users to be sources of interference. After decoding the common message, the qth user focuses on extracting its private message. The SINR for this private message reflects the power allotted to specific data of the user relative to the interference caused by private messages intended for other users, along with residual channel estimation errors and noise. This equation is crucial as it determines the reliability of personalized data delivery, highlighting the trade-off in power allocation between private and common messages in RSMA. Thereby, the SINR for the qth user to successfully decode their private message can be articulated as:

$$\bar{\gamma}_{p,q} = \frac{a_q \mathcal{A}_q}{\mathcal{A}_q \sum_{j=1, q \neq j}^{Q} a_j + \delta_q \mu_{U_q}^2 + 1}$$

(6)

Owing to identical power transmission associated with L training symbols utilized for channel estimation, $\mu_{U_q}^2 = 1 / \delta_q L$ is modeled as the variance of channel estimation error [21].

2.3. Terrestrial channel model

Assuming independent and identically distributed (IID) fading channels yields the probability density function (PDF) of $g_q^{(k)}$ expressed to be:

$$f_{\left|g_q^{(k)}\right|^2}(x) = \alpha_q e^{-\beta_q x} {}_1F_1\left(m_q; 1; \varpi_q x\right) \quad , x \geq 0$$

(7)

wherein ${}_1F_1\left(\cdot; \cdot; \cdot\right)$ means the confluent hypergeometric function of the first kind [22]. Moreover, $g_q^{(k)}, \forall q \in Q$, is channel coefficient from satellite's kth antenna to qth user, $\beta_q = 1/2b_q, \alpha_q = \left(2b_q m_q / \left(2b_q m_q + \Omega_q\right)\right)^{m_q} / 2b_q$, $\varpi_q = \Omega_q / \left(2b_q\right)\left(2b_q m_q + \Omega_q\right)$ in which $2b_q$, Ω_q, and m_q represents average power of multi-path elements, average power of line-of-sight element, and fading severity parameter, correspondingly.

For the purposes of this paper, the shadowed-Rician fading severity parameter m_q is assumed to be integer values. This assumption facilitates a streamlined evaluation of channel characteristics and their influence on performance indicators. We now reformulate (7) as:

$$f_{\left|g_q^{(k)}\right|^2}(x) = \alpha_q e^{-(\beta_q - \varpi_q)x} \sum_{t=0}^{m_q - 1} \zeta_q(t) x^t \quad , x \geq 0$$

(8)

Here, $\zeta_q(t) = (-1)^t (1 - m_q)_t \varpi_q^t / (t!)^2$, where $(.)_t$ represents the Pochhammer symbol. Drawing on the findings from [23], the probability density function (PDF) of $\mathcal{A}_q$ under i.i.d. shadowed-Rician fading is expressed as:

$$f_{\mathcal{A}_q}(x) = \sum_{j_1=0}^{m_q - 1} \cdots \sum_{j_K=0}^{m_q - 1} \frac{\Lambda_q(K)}{\delta_q^{\Delta_q}} x^{\Delta_q - 1} e^{-\left(\frac{\psi_q}{\delta_q}\right)x}$$

(9)

where $\Delta_q = \sum_{l=1}^{K} j_l + K$, $\psi_q = \beta_q - \delta_q$, $\mathcal{B}(.,.)$ means the Beta function [22], and

$$\Lambda_q(K) = \alpha_q^K \prod_{l=1}^{K} \zeta_q(j_l) \prod_{u=1}^{K-1} \mathcal{B}\left(\sum_{p=1}^{u} j_p + u, j_{u+1} + 1\right) \tag{10}$$

To obtain the CDF of $\mathcal{A}$, we utilize the findings from [22], resulting in $F_{\mathcal{A}_q}(x)$ expressed as:

$$F_{\mathcal{A}_q}(x) = 1 - \sum_{j_1=0}^{m_q-1} \cdots \sum_{j_K=0}^{m_q-1} \sum_{p=0}^{\Delta_q-1} \frac{\Lambda_q(K)\Gamma(\Delta_q)}{p!\psi_q^{\Delta_q-p}\delta_q^p} e^{-\frac{\psi_q x}{\delta_q}} x^p \tag{11}$$

3. OUTAGE PROBABILITY

It is recalled from RSMA that every user gets the mix of the shared information, its own private information, the private information of all other users. Thereby, it decodes both types of information through a two-stage recovering process, as shown in (5) and (6). If these SINRs drop below the required thresholds $\gamma_{th}^{c,q}$ and $\gamma_{th}^{p,q}$, respectively, the connection between S and the qth user will experience an outage. Here, $\gamma_{th}^{c,q} = 2^{2R_{c,q}} - 1$ and $\gamma_{th}^{p,q} = 2^{2R_{p,q}} - 1$, where $R_{p,q}$ and $R_{c,q}$ denote preset spectral efficiencies to restore private and common information, correspondingly.

The outage probability (OP) for the qth user quantifies the likelihood that the SINR for either the private or common message falls below the required threshold, leading to a communication failure. This equation combines the effects of channel conditions, power allocation, and fading characteristics under shadowed-Rician fading. It distinguishes between cases where the common or private message decoding is the limiting factor, providing a comprehensive metric to evaluate system reliability and guide optimization of power allocation and antenna configurations.

Proposition 1 The OP for the qth user is:

$$\mathcal{O}_{U_q} = \begin{cases} 1 - \sum_{j_1=0}^{m_q-1} \cdots \sum_{j_K=0}^{m_q-1} \sum_{p=0}^{\Delta_q-1} \frac{\Lambda_q(K)\Gamma(\Delta_q)}{p!\psi_q^{\Delta_q-p}\delta_q^p} e^{-\frac{\psi_q \gamma_{th}^{p,q}\left(\delta_q \mu_{U_q}^2+1\right)}{\delta_q\left[a_q-(1-a_c-a_q)\gamma_{th}^{p,q}\right]}} \left(\frac{\gamma_{th}^{p,q}\left(\delta_q \mu_{U_q}^2+1\right)}{a_q-(1-a_c-a_q)\gamma_{th}^{p,q}}\right)^p & , if\ \bar{\gamma}_{th}^{c,q} < \bar{\gamma}_{th}^{p,q} \\ 1 - \sum_{j_1=0}^{m_q-1} \cdots \sum_{j_K=0}^{m_q-1} \sum_{p=0}^{\Delta_q-1} \frac{\Lambda_q(K)\Gamma(\Delta_q)}{p!\psi_q^{\Delta_q-p}\delta_q^p} e^{-\frac{\psi_q \gamma_{th}^{c,q}\left(\delta_q \mu_{U_q}^2+1\right)}{\delta_q\left[a_c-(1-a_c)\gamma_{th}^{c,q}\right]}} \left(\frac{\gamma_{th}^{c,q}\left(\delta_q \mu_{U_q}^2+1\right)}{a_c-(1-a_c)\gamma_{th}^{c,q}}\right)^p & , if\ \bar{\gamma}_{th}^{c,q} \geq \bar{\gamma}_{th}^{p,q} \end{cases} \tag{12}$$

where $\bar{\gamma}_{th}^{c,q} = \gamma_{th}^{c,q}\left(\delta_q \mu_{U_q}^2 + 1\right)/(a_c - (1-a_c)\gamma_{th}^{c,q})$ and $\bar{\gamma}_{th}^{p,q} = \gamma_{th}^{p,q}\left(\delta_q \mu_{U_q}^2 + 1\right)/(a_q - (1-a_c-a_q)\gamma_{th}^{p,q})$. Note (12) is derived on the condition of $a_c > \gamma_{th}^{c,q}/(1+\gamma_{th}^{c,q})$ and $a_i > (1-a_c)\gamma_{th}^{p,q}/(1+\gamma_{th}^{p,q})$.

Proof 1 The OP for the qth user is expressed as:

$$\mathcal{O}_{U_q} = 1 - \Pr\left(\bar{\gamma}_{c,q} > \gamma_{th}^{c,q}, \bar{\gamma}_{p,q} > \gamma_{th}^{p,q}\right)$$
$$= 1 - \Pr\left(\frac{a_c\mathcal{A}_q}{(1-a_c)\mathcal{A}_q + \delta_q \mu_{U_q}^2 + 1} > \gamma_{th}^{c,q}, \frac{a_q\mathcal{A}_q}{\mathcal{A}_q \sum_{j=1,q\neq j}^{Q} a_j + \delta_q \mu_{U_q}^2 + 1} > \gamma_{th}^{p,q}\right) \tag{13}$$

After certain algebraic simplifications, the (13) is represented as:

$$\mathcal{O}_{U_q} = 1 - \Pr\left(\mathcal{A}_q > \bar{\gamma}_{th}^{c,q}, \mathcal{A}_q > \bar{\gamma}_{th}^{p,q}\right) = 1 - \Pr\left(\mathcal{A}_q > \bar{\gamma}_{\max}^q\right), \tag{14}$$

where $\bar{\gamma}_{\max}^q = \max\left(\bar{\gamma}_{th}^{c,q}, \bar{\gamma}_{th}^{p,q}\right)$. Further, we rewrite $\mathcal{O}_{U_q}$ as:

$$\mathcal{O}_{U_q} = 1 - \left[1 - F_{\mathcal{A}_q}\left(\bar{\gamma}_{\max}^q\right)\right] = F_{\mathcal{A}_q}\left(\bar{\gamma}_{\max}^q\right) \tag{15}$$

Substituting (11) into (15), (12) can be obtained and the proof is completed.

When $\varrho_S \to \infty$, one applies the approximation $e^{-z} \approx 1 - z$ as [24] into (13) to achieve the approximated CDF of $\mathcal{A}_q$, yielding asymptotic behavior as:

$$F_{\mathcal{A}_q}^{\infty}(x) \simeq \frac{\alpha_q^K x^K}{K!\delta_q^K} \tag{16}$$

Substituting (16) into (15) results in the asymptotic OP at U_q as:

$$\mathcal{O}_{U_q}^{\infty} = \begin{cases} \frac{1}{K!} \left\langle \frac{\alpha_q \gamma_{th}^{p,q} \left(\delta_q \mu_{U_q}^2 + 1 \right)}{\delta_q \left[a_q - (1 - a_c - a_q) \gamma_{th}^{p,q} \right]} \right\rangle^K & , if \ \bar{\gamma}_{th}^{c,q} < \bar{\gamma}_{th}^{p,q} \\ \frac{1}{K!} \left\langle \frac{\alpha_q \gamma_{th}^{c,q} \left(\delta_q \mu_{U_q}^2 + 1 \right)}{\delta_q \left[a_c - (1 - a_c) \gamma_{th}^{c,q} \right]} \right\rangle^K & , if \ \bar{\gamma}_{th}^{c,q} \geq \bar{\gamma}_{th}^{p,q} \end{cases} \quad (17)$$

4. PERFORMANCE EVALUATION

This section presents demonstrative findings to validate the proposed formulas. The shadowed-Rician fading configuration for the satellite to qth user (S-U_q) connection is considered as $\Omega_q, m_q, b_q = 0.279, 5, 0.251$ in average shadowing (AS) scenario and ($\Omega_q, m_q, b_q = 0.0007, 1, 0.063$) under heavy shadowing (HS) in [25]. The equivalent noise power at U_q is calculated as $\sigma_q^2 = N_0 + 10 \log_{10}(W) + \text{NF}$ [dBm], as referenced in [26], where NF is noise figure. Unless otherwise stated in [20], the parameters are set to $K = 2, Q = 2, R_{c,q} = 0.1$ bits per channel usage (BPCU), $R_{p,1} = 0.25$ BPCU, $R_{p,2} = 0.1$ BPCU, $a_c = 0.4, f_c = 2$ GHz, $W = 15$ Mhz, $T = 300°K, c = 3 \times 10^8$ m/s, $d_{SU_q} = 35786$ Km, $\vartheta_S = 53.45$ dB, $\vartheta_{U_q} = 4.8$ dB, $\theta_{U_q} = 0.8°, \theta_{U_q 3dB} = 0.3°$, NF = 10 dBm, $N_0 = -174$ dBm/Hz, $a_2 = 0.4(1 - a_c), a_1 = 0.6(1 - a_c)$, with BPCU representing bits per channel use.

Figure 2 illustrates OP versus satellite transmits power P_S in dBm. It compares analytical results (for both HS and AS conditions) with simulation results and asymptotic expressions. The curves for U_1 and U_2 under HS and AS conditions show a close match between the analytical and simulation findings, validating the accuracy of the analysis. Furthermore, the asymptotic expressions provide a good approximation at higher values of P_S, highlighting the advantage of the proposed model. This also indicates the significant influence of shadowing severity on the OP of satellite communications systems.

Figure 3 presents OP against satellite transmit power P_S in dBm for numerous numbers of satellite antennas K, specifically $K = 1, 2, 3$. The analytical curves for U_1 and U_2 closely match the simulation outcomes, confirming the preciseness of the analysis. As K increases, the OP decreases for a given P_S, highlighting the advantage of using multiple antennas in satellite systems to enhance reliability. For instance, at higher P_S, the performance improvement is more prominent due to the additional spatial diversity offered by the rising quantity of antennas. The asymptotic curves also align well at higher power levels, further validating the robustness of the derived expressions under high transmit power scenarios.

Figure 4 illustrates OP versus power coefficient a_c for two satellite transmit power levels: $P_S = 0$ dBm (dashed lines) and $P_S = 5$ dBm (solid lines). The analytical results for U_1 and U_2 closely align with the simulation outcomes, validating the analysis. The OP exhibits a U-shaped behavior, decreasing as a_c increases from 0, reaching a minimum near $a_c = 0.5$, and then increasing as a_c approaches 1. This behavior highlights the trade-off in power allocation between the users, where balanced power allocation ($a_c \approx 0.5$) minimizes the OP. Furthermore, higher satellite power ($P_S = 5$ dBm) consistently results in lower outage probabilities compared to $P_S = 0$ dBm, demonstrating the advantage of increased transmit power. The figure also emphasizes the importance of optimizing a_c to enhance system performance under varying power levels.

Figure 5 presents OP versus the lengths of training symbols L with $P_S = 0$ dBm for $K = 1$ (dashed lines) and $K = 3$ (solid lines). This figure demonstrates that the OP of U_1 is consistently below that of U_2, indicating that U_1 experiences better information quality compared to U_2. Additionally, the case with $K = 1$ exhibits higher OP compared to $K = 3$. This observation implies that rising the quantity of antennas enhances the communication quality and efficiency.

Figure 6 clearly illustrates that RSMA consistently outperforms NOMA in reducing OP for both users across all transmit power levels. Under HS, RSMA's curves decrease more rapidly, demonstrating robust reliability even at low PS, whereas NOMA sustains higher outage probabilities. The AS further amplifies RSMA's advantage, reducing its OP to extremely low values more quickly than NOMA. User 1 consistently experiences a lower OP than User 2, reflecting superior channel conditions and RSMA's ability to exploit this disparity. As PS increases from –25 dBm to +5 dBm, all curves decline; however, RSMA maintains a distinct advantage over NOMA, underscoring its resilience to shadowing. Overall, Figure 6 clearly demonstrates that RSMA provides a more reliable link under both HS and AS, establishing it as the superior approach for next-generation satellite communications.
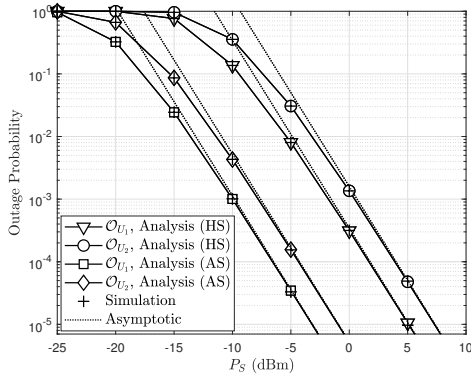
Figure 2. Outage probability versus P_S under various shadow fading, with $L = 5$
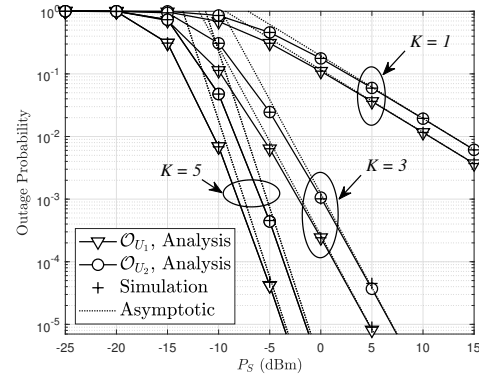

Figure 3. Outage probability versus P_S and the numbers of antennas of the satellite, with $L = 10$
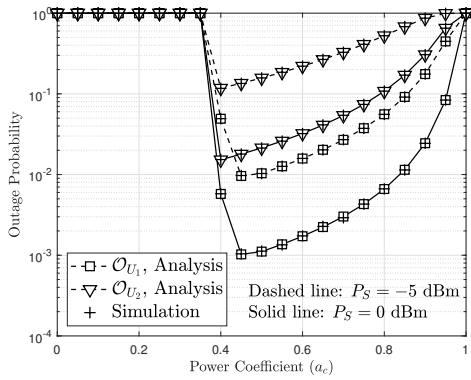

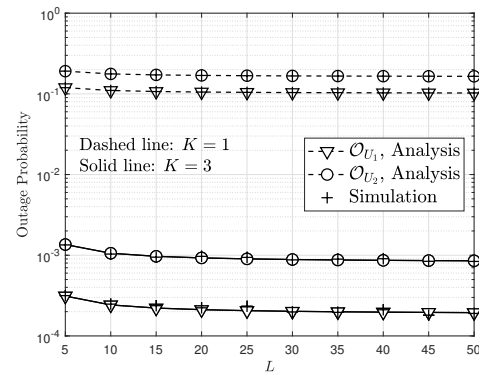Figure 4. OP against a_c with $K = 2$ and $L = 20$
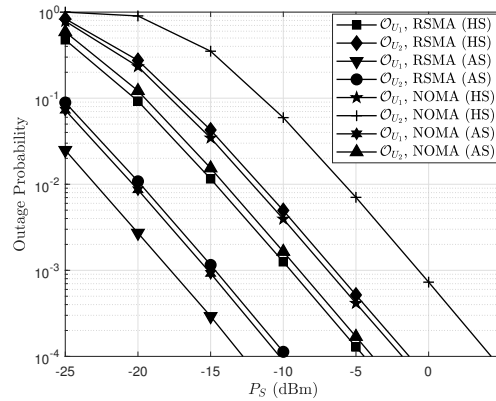

Figure 5. OP versus L with $P_S = 0$ dBm

Figure 6. Comparison between RSMA and NOMA for the outage probability versus P_S with $K = 2$ and $L = 5$

5. CONCLUSION

This study leverages the integration of RSMA into satellite-terrestrial communication systems to significantly enhance quality of service. By deriving mathematical expressions for outage probability and con-

ducting asymptotic analysis, the research underscores the critical roles of satellite antenna configuration and optimized power distribution in enhancing communication reliability. Numerical simulation validates the accuracy of the theoretical findings, demonstrating that RSMA reduces outage probability by up to 20% compared to NOMA under heavy shadowing conditions, owing to its superior interference management and flexible signal decoding capabilities. The results highlight the efficacy of employing multiple antennas and balanced power allocation (e.g., $a_c \approx 0.5$) to minimize outage probability and enhance reliability, particularly in challenging propagation environments. The study provides practical guidelines for optimizing satellite-terrestrial networks, such as increasing the number of satellite antennas to exploit spatial diversity and carefully tuning power allocation coefficients to balance common and private message transmission. Future research directions include exploring RSMA's applicability in dynamic environments, such as low earth orbit (LEO) satellite systems, which offer lower latency but introduce challenges like rapid handovers and Doppler effects. Additionally, integrating RSMA with 6G edge networks could further enhance performance by leveraging edge computing for real-time interference management and resource allocation. Further investigations should also focus on improving energy efficiency, reducing latency, and ensuring scalability to support the growing demands of next-generation wireless networks.

ACKNOWLEDGMENT

FUNDING INFORMATION

AUTHOR CONTRIBUTIONS STATEMENT

This journal uses the Contributor Roles Taxonomy (CRediT) to recognize individual author contributions, reduce authorship disputes, and facilitate collaboration.

Name of Author	C	M	So	Va	Fo	I	R	D	O	E	Vi	Su	P	Fu
Huu Q. Tran	✓	✓		✓	✓	✓		✓	✓	✓				
Khuong Ho-Van		✓				✓		✓		✓				

C	: **C**onceptualization	I	: **I**nvestigation	Vi	: **Vi**sualization
M	: **M**ethodology	R	: **R**esources	Su	: **Su**pervision
So	: **So**ftware	D	: **D**ata Curation	P	: **P**roject Administration
Va	: **Va**lidation	O	: Writing - **O**riginal Draft	Fu	: **Fu**nding Acquisition
Fo	: **Fo**rmal Analysis	E	: Writing - Review & **E**diting		

CONFLICTS OF INTEREST

The authors declare no conflict of interest in this manuscript.

INFORMED CONSENT

We have obtained informed consent from all individuals included in this study.

ETHICAL APPROVAL

Not applicable.

DATA AVAILABILITY

Data availability is not applicable to this paper as no new data were created or analyzed in this study.

REFERENCES

[1] X. Huang, K. Niu, Z. Si, Z. He, and C. Dong, "Rate-Splitting Non-orthogonal Multiple Access: Practical Design and Performance Optimization," *Communications and Networking. ChinaCom 2016, Q. Chen, W. Meng, and L. Zhao, Eds., Lecture Notes of the Institute for Computer Sciences, Social Informatics and Telecommunications Engineering*, vol. 209. Cham, Switzerland: Springer, pp. 349-359, 2018, doi: 10.1007/978-3-319-66625-9_34.

[2] Y. Mao, B. Clerckx, and V. O. K. Li, "Rate-splitting multiple access for downlink communication systems: bridging, generalizing, and outperforming SDMA and NOMA," *EURASIP Journal on Wireless Communications and Networkin*, vol. 2018, no. 133, 2018, doi: 10.1186/s13638-018-1104-7.

[3] Y. Mao, O. Dizdar, B. Clerckx, R. Schober, P. Popovski and H. V. Poor, "Rate-Splitting Multiple Access: Fundamentals, Survey, and Future Research Trends," *IEEE Communications Surveys & Tutorials*, vol. 24, no. 4, pp. 2073-2126, 2022, doi: 10.1109/COMST.2022.3191937.

[4] B. Clerckx *et al.*, "A Primer on Rate-Splitting Multiple Access: Tutorial, Myths, and Frequently Asked Questions," *IEEE Journal on Selected Areas in Communications*, vol. 41, no. 5, pp. 1265-1308, May 2023, doi: 10.1109/JSAC.2023.3242718.

[5] S. Jang, N. Kim, G. Kim, and B. Lee, "Recent Trend of Rate-Splitting Multiple Access-Assisted Integrated Sensing and Communication Systems," *Electronics*, vol. 13, no. 23, PP. 4579, 2024, doi: 10.3390/electronics13234579.

[6] L. Yin and B. Clerckx, "Rate-Splitting Multiple Access for Satellite-Terrestrial Integrated Networks: Benefits of Coordination and Cooperation," *IEEE Transactions on Wireless Communications*, vol. 22, no. 1, pp. 317-332, Jan. 2023, doi: 10.1109/TWC.2022.3192980.

[7] J. Park *et al.*, "Rate-Splitting Multiple Access for 6G Networks: Ten Promising Scenarios and Applications," *IEEE Network*, vol. 38, no. 3, pp. 128-136, May 2024, doi: 10.1109/MNET.2023.3321518.

[8] H. Tang, X. Sun, L. Yang, G. Hu, and Z. Zhong, "Energy Minimization for Low-Latency Downlink Rate Splitting Multiple Access," *Energy Minimization for Low-Latency Downlink Rate Splitting Multiple Access. In: Qin, Y., Jia, L., Yang, J., Diao, L., Yao, D., An, M. (eds) Proceedings of the 6th International Conference on Electrical Engineering and Information Technologies for Rail Transportation (EITRT) 2023. EITRT 2023. Lecture Notes in Electrical Engineering*, vol. 1137. Singapore: Springer, 2024, doi: 10.1007/978-981-99-9311-6_43.

[9] A.-T. Tran, D. S. Lakew, D. T. Hua, Q. T. Do, N.-N. Dao, and S. Cho, "A Review on Rate-Splitting Multiple Access-Assisted Downlink Networks: Rate Optimizations," *2023 International Conference on Information Networking (ICOIN)*, Bangkok, Thailand, pp. 534–536, 2023, doi: 10.1109/ICOIN56518.2023.10049025.

[10] X. Sheng, "Effective Capacity of Rate-Splitting Multiple Access with Channel Estimation Errors." *Physical Communication*, vol. 64, pp. 102331, 2024, doi: 10.1016/j.phycom.2024.102331.

[11] Z. Lin, M. Lin, B. Champagne, W. -P. Zhu and N. Al-Dhahir, "Secure and Energy Efficient Transmission for RSMA-Based Cognitive Satellite-Terrestrial Networks," *IEEE Wireless Communications Letters*, vol. 10, no. 2, pp. 251-255, Feb. 2021, doi: 10.1109/LWC.2020.3026700.

[12] S. Zhang, S. Zhang, W. Yuan, Y. Li and L. Hanzo, "Efficient Rate-Splitting Multiple Access for the Internet of Vehicles: Federated Edge Learning and Latency Minimization," *IEEE Journal on Selected Areas in Communications*, vol. 41, no. 5, pp. 1468-1483, May 2023, doi: 10.1109/JSAC.2023.3240716.

[13] Q. Zhang, L. Zhu, Y. Chen, and S. Jiang, "Constrained DRL for Energy Efficiency Optimization in RSMA-Based Integrated Satellite Terrestrial Network," *Sensors*, vol. 23, no. 18, pp. 7859, 2023. doi: 10.3390/s23187859.

[14] A. Mishra, Y. Mao, O. Dizdar and B. Clerckx, "Rate-Splitting Multiple Access for 6G—Part I: Principles, Applications and Future Works," *IEEE Communications Letters*, vol. 26, no. 10, pp. 2232-2236, Oct. 2022, doi: 10.1109/LCOMM.2022.3192012.

[15] J. Shi, H. Yang, X. Chen, and Z. Yang, "Resource allocation for integrated satellite-terrestrial networks based on RSMA," *IET Communications*, pp. 1–12, 2024, doi: 10.1049/cmu2.12745.

[16] H. Zhang, M. Chen, A. Vahid, and F. Ye, H. Sun, "Model-based Deep Learning for QoS-Aware Rate-Splitting Multiple Access Wireless Systems," *arXiv.*, 2014, doi: 10.48550/arXiv.2411.03507.

[17] A. Arcidiacono, D. Finocchiaro, R. De Gaudenzi, O. del Rio-Herrero, S. Cioni, M. Andrenacci, and R. Andreotti, "Is Satellite Ahead of Terrestrial in Deploying NOMA for Massive Machine-Type Communications?," *Sensors*, vol. 21, no. 13, pp. 4290, 2021, doi: 10.3390/s21134290.

[18] J. Arnau, D. Christopoulos, S. Chatzinotas, C. Mosquera and B. Ottersten, "Performance of the Multibeam Satellite Return Link With Correlated Rain Attenuation," *IEEE Transactions on Wireless Communications*, vol. 13, no. 11, pp. 6286-6299, Nov. 2014, doi: 10.1109/TWC.2014.2329682.

[19] X. Li *et al.*, "Security and Reliability Performance Analysis of Cooperative Multi-Relay Systems With Nonlinear Energy Harvesters and Hardware Impairments," *IEEE Access*, vol. 7, pp. 102644-102661, 2019, doi: 10.1109/ACCESS.2019.2930664.

[20] P. K. Sharma, D. Deepthi and D. I. Kim, "Outage Probability of 3-D Mobile UAV Relaying for Hybrid Satellite-Terrestrial Networks," *IEEE Communications Letters*, vol. 24, no. 2, pp. 418-422, Feb. 2020, doi: 10.1109/LCOMM.2019.2956526.

[21] J. Zhao, X. Yue, S. Kang and W. Tang, "Joint Effects of Imperfect CSI and SIC on NOMA Based Satellite-Terrestrial Systems," *IEEE Access*, vol. 9, pp. 12545-12554, 2021, doi: 10.1109/ACCESS.2021.3051306.

[22] I. S. Gradshteyn, I. M. Ryzhik, A. Jeffrey, and D. Zwillinger, *Table of Integrals, Series and Products*, 7th ed. Boston, MA, USA: Elsevier, 2007.

[23] V. Bankey, P. K. Upadhyay, D. B. Da Costa, P. S. Bithas, A. G. Kanatas and U. S. Dias, "Performance Analysis of Multi-Antenna Multiuser Hybrid Satellite-Terrestrial Relay Systems for Mobile Services Delivery," *IEEE Access*, vol. 6, pp. 24729-24745, 2018, doi: 10.1109/ACCESS.2018.2830801.

[24] K. Guo *et al.*, "Power Allocation and Performance Evaluation for NOMA-Aided Integrated Satellite-HAP-Terrestrial Networks Under Practical Limitations," *IEEE Internet of Things Journal*, vol. 11, no. 7, pp. 13002-13017, 1 April1, 2024, doi: 10.1109/JIOT.2023.3337124.

[25] N. I. Miridakis, D. D. Vergados and A. Michalas, "Dual-Hop Communication Over a Satellite Relay and Shadowed Rician Channels," *IEEE Transactions on Vehicular Technology*, vol. 64, no. 9, pp. 4031-4040, Sept. 2015, doi: 10.1109/TVT.2014.2361832.

[26] H. Q. Tran and B. M. Lee, "RIS-NOMA-assisted short-packet communication with direct links," *Journal of King Saud University-Computer and Information Sciences*, vol. 36, no. 3, pp. 101979, 2024, doi: 10.1016/j.jksuci.2024.101979.

BIOGRAPHIES OF AUTHORS

Huu Q. Tran ⬛🔗🆔 (Member, IEEE) received the M.S. degree in Electronics Engineering from Ho Chi Minh City University of Technology and Education (HCMUTE), Vietnam in 2010. Currently, he has been working as a lecturer at Faculty of Electronics Technology, Industrial University of Ho Chi Minh City (IUH), Vietnam. He obtained his doctorate from the Faculty of Electrical and Electronics Engineering at HCMUTE, Vietnam. His research interests include wireless communications, non-orthogonal multiple access (NOMA), energy harvesting (EH), wireless cooperative relaying networks, heterogeneous networks (HetNet), cloud radio access networks (C-RAN), unmanned aerial vehicles (UAV), reconfigurable intelligent surfaces (RIS), short-packet communication (SPC) and internet of things (IoT). He can be contacted at email: tranquyhuu@iuh.edu.vn.

Khuong Ho-Van ⬛🔗🆔 (Member, IEEE) received the B.E. (first-ranked honor) and M.S. degrees in Electronics and Telecommunications Engineering from Ho Chi Minh City University of Technology, Vietnam, in 2001 and 2003, respectively, and the Ph.D. degree in Electrical Engineering from the University of Ulsan, South Korea, in 2007. From 2007 to 2011, he joined McGill University, Canada, as a Postdoctoral Fellow. Currently, he is an Associate Professor with Ho Chi Minh City University of Technology, Vietnam. His major research interests include modulation and coding techniques, diversity techniques, digital signal processing, energy harvesting, physical layer security, and cognitive radio. He can be contacted at email: hvkhuong@hcmut.edu.vn.